Supporting Material for "Nonequilibrium dissipation-free transport in F1-ATPase and the thermodynamic role of asymmetric allosterism"

Kyogo Kawaguchi*, Shin-ichi Sasa†, and Takahiro Sagawa‡

*Department of Physics, The University of Tokyo, Bunkyo-ku, Tokyo, 113-0033, Japan
†Department of Physics, Kyoto University, Sakyo-ku, Kyoto 606-8502, Japan
‡Department of Basic Science, The University of Tokyo, Meguro-ku, Tokyo 153-8902, Japan

A. Effective potential in the fast chemical reaction limit

Here we show that by assuming fast ATP hydrolysis and Pi release, the dynamics apart from the slow 120° steps are governed by the overdamped Brownian motion inside the effective potentials $U_i(x)$. Through the same method, we may prove that in the high ATP concentration limit, one obtains the tilted periodic potential picture (Fig. 2*C* in the main text) for the full dynamics.

We consider that there are two potentials (Fig. S1), $U_{\mathrm{h}}(x)$ and $U_{\mathrm{b}}(x)$, corresponding to the ATP hydrolysis dwell (centered at $x=-l=-40°$) and the ATP binding dwell ($x=0$). To neglect the slow switching (80° step), we assume that the probe is contained in either of the potential for the time scale of interest. We assume that the potential energy is large compared to the thermal energy, $U_{\mathrm{h}}(0), U_{\mathrm{h}}(-l) \gg k_{\mathrm{B}}T$, which is the case observed in experiment. Let $P_{\mathrm{h}}^{t}(x)$ and $P_{\mathrm{b}}^{t}(x)$ be the probability density functions of finding x inside each potentials. The Fokker-Planck equations read

$$\frac{\partial}{\partial \tilde{t}} P_i^{\tilde{t}}(x) = \frac{k_{\mathrm{B}}T}{\Gamma X l_v^2}\frac{\partial}{\partial \tilde{x}}\left[\frac{d\tilde{U}_i(x)}{d\tilde{x}} P_i^{\tilde{t}}(\tilde{x}) + \frac{\partial}{\partial \tilde{x}} P_i^{\tilde{t}}(\tilde{x})\right] + f_j(\tilde{x}) P_j^{\tilde{t}}(\tilde{x}) - f_i(\tilde{x}) P_i^{\tilde{t}}(\tilde{x}) \qquad \text{(S1)}$$

where i and j , i are h or b. We have normalized the equation using $\tilde{t}=Xt$, $\tilde{x}=x/l_v$, and $\tilde{U}_{\mathrm{i}}(x)=U_i(x)/k_{\mathrm{B}}T$. Here, X is the typical (slowest) rate of the ATP hydrolysis or the Pi releasing reaction. As the typical length scale l_v, we shall adopt the length scale of $E(x):=[U_{\mathrm{h}}(x)-U_{\mathrm{b}}(x)+\Delta\mu]/k_{\mathrm{B}}T$, which is much smaller than the length scale of $U_{\mathrm{h}}(x)$ in the large potential energy setup. The switching rates from h to b and b to h have been defined as $Xf_{\mathrm{h}}(x)$ and $Xf_{\mathrm{b}}(x)$, respectively, which satisfy the local detailed balance:

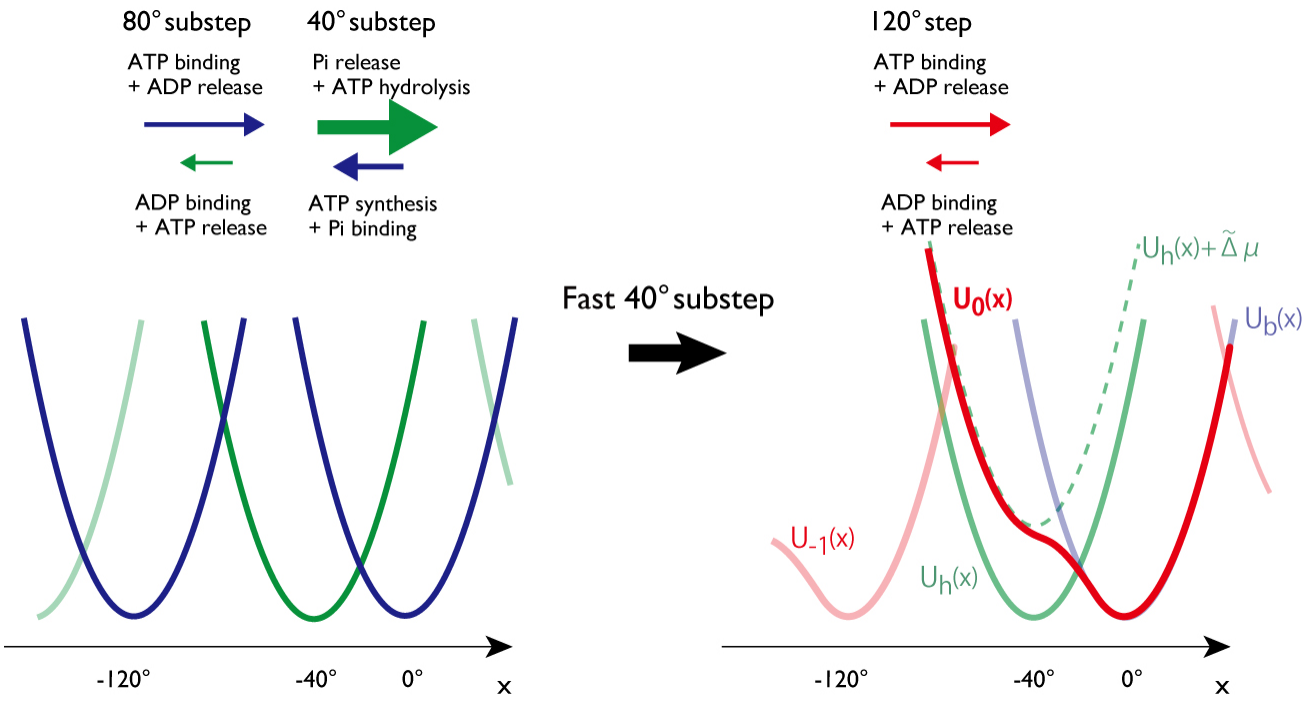

FIGURE S1 Left: Mechanical potentials and chemical reactions corresponding to the substeps. Right: In the limit of the fast 40° substep, the two potentials, $U_{\mathrm{h}}(x)$ and $U_{\mathrm{b}}(x)$, corresponding to the ATP hydrolysis dwell and the ATP binding dwell, respectively, will be merged into one effective potential, $U_0(x)$. When $U_{\mathrm{h}}(x)$ and $U_{\mathrm{b}}(x)$

are assumed to be harmonic with the same spring constant (as observed in [1]), $U_0(x)$ is given by Eq. S7. Numerical results presented in the main text were obtained using this $U_0(x)$.

$$\frac{f_{\mathrm{h}}(x)}{f_{\mathrm{b}}(x)} = \exp\left\{-\frac{[U_{\mathrm{h}}(x) - U_{\mathrm{b}}(x) + \Delta\mu]}{k_{\mathrm{B}}T}\right\}. \tag{S2}$$

The free energy difference between the ATP bound state and the ATP hydrolyzed + Pi released state of the F_1 is denoted as $\tilde{\Delta}\mu$. Assuming fast reaction ($X \to \infty$) corresponds to taking $\epsilon := 1/\tau_v X$ as the small parameter, where $\tau_v := \Gamma l_v^2/k_{\mathrm{B}}T$. Let us calculate $P_i^t(x)$ in the form, $P_i^t(x) = P_i^{(0)}(x) + \epsilon P_i^{(1)}(x) + O(\epsilon^2)$. We obtain from the 0-th order equations in Eq. S1:

$$P_i^{(0)}(x) = Q^t(x)P_i^*(x), \tag{S3}$$

where $P_{\mathrm{h}}^*(x) = \{1 + \exp[E(x)]\}^{-1}$ and $P_{\mathrm{b}}^*(x) = \{1 + \exp[-E(x)]\}^{-1}[= 1 - P_{\mathrm{h}}(x)]$. We adopted the length scale of $E(x)$ as l_v in Eq. S1 since this is the length scale of $P_{\mathrm{h,b}}(x)$ which is critical in the perturbation theory. The solvability condition for the 1st order equations in Eq. S1 determines the dynamics of $Q^t(x)$:

$$\frac{\partial}{\partial t}Q^t(x) = \frac{1}{\Gamma}\frac{\partial}{\partial x}\left[\sum_{i=\mathrm{h,b}} P_i^*(x)\frac{dU_i(x)}{dx}Q^t(x) + k_{\mathrm{B}}T\frac{\partial}{\partial x}Q^t(x)\right] \tag{S4}$$

which is equivalent to the one-dimensional overdamped Langevin equation with the effective force

$$-\frac{dU_0(x)}{dx} = -\sum_{i=\mathrm{h,b}} P_i^*(x)\frac{dU_i(x)}{dx} \tag{S5}$$

where the effective potential is obtained by

$$U_0(x) = \int_c^x dx \sum_{i=\mathrm{h,b}} P_i^*(x)\frac{dU_i(x)}{dx} \tag{S6}$$

with an arbitrary fixed constant c (Fig. S1). Assuming that the two potentials $U_{\mathrm{h}}(x)$ and $U_{\mathrm{b}}(x)$ are harmonic with the same spring constants, $U_{\mathrm{b}}(x) = U_{\mathrm{h}}(x + l) = kx^2/2$, which is consistent with the ATP binding dwell and catalytic dwell observed in experiment [1], we have an explicit form

$$U_0(x) = k_{\mathrm{B}}T\left[\frac{1}{2}kx^2 + \log\left[e^{-klx} + e^{\tilde{\Delta}\mu/k_{\mathrm{B}}T + kl^2/2}\right]\right] \tag{S7}$$

We used Eq. S7 to fit the potential estimated from the probe trajectory [4] by the parameters k and $\Delta\tilde{\mu}$, and obtained $k = 0.0061\ \mathrm{deg}^{-2}k_{\mathrm{B}}T$. and $\tilde{\Delta}\mu = 5.2\ k_{\mathrm{B}}T$.

The high ATP concentration case of the full dynamics [which consists of potentials $U_n(x)$ and switching rates $R_n^{\pm}(x)$] could be treated in a similar manner if we adopt as l_v the length scale of $E_n(x) := [U_n(x) - U_{n+1}(x) + \Delta\mu]/k_{\mathrm{B}}T$ and consider the limit $W\tau_v \gg 1$. The dynamics in this limit is described by

$$\Gamma\dot{x} = F(x) + \sqrt{2\Gamma k_{\mathrm{B}}T}\xi_t \tag{S8}$$

The effective force $F(x)$ is given by

$$F(x) = \sum_{n=-\infty}^{\infty} P_n^*(x)\frac{dU_n(x)}{dx} \tag{S9}$$

with $P_n^*(x)$ defined similarly to the previous case as

$$P_n^*(x) := \frac{\exp\{-[U_n(x) - n\Delta\mu]/k_BT\}}{\sum_{m=-\infty}^{\infty}\exp\{-[U_m(x) - m\Delta\mu]/k_BT\}} \tag{S10}$$

The force in Eq. S9 corresponds to a tilted periodic potential, where the energy difference per 120° step is $\Delta\mu$ (Fig. 2*B*). Since this energy difference is dissipated through the rotational motion of the probe,

$$Q_{\mathrm{ext}} := -\int_{0^\circ}^{120^\circ} F(x)dx = \Delta\mu\,. \tag{S11}$$

The maximum velocity v, which is the steady-state velocity of the model described by Eq. S8, may be obtained analytically using $F(x)$.

B. Harmonic potential model

We consider in this section the simplified harmonic potential case, $U_n(x) = K(x - nL)^2/2$, with $L = 120°$. In Fig. S2, we show the numerical results of Q_{ext} in this model. Under the condition that the diffusion coefficient $D = k_BT/\Gamma$ as $D/L^2 = 3.3\ \text{sec}^{-1}$ [4], and the chemical potential as $\Delta\mu/k_BT = 19$ [5, 6], the value of K was determined as $KL^2/k_BT = 50$ by setting the maximum average velocity to fit with that obtained in experiment. The characteristic feature of q dependence is similar to the case of Fig. 2*C*, where the potential estimated through experiment was used in the calculation. Note that in this model, the angular position dependence of the forward switching rate has a simple form,

$$R_n^+(x) \propto \exp[qKLx/k_BT] \tag{S12}$$

which allows us to directly compare the value of q with the experimentally observed rates of ATP binding[1, 2, 3]. Using the above parameters, we obtain $q = 0.07 \sim 0.1, 0.11,$ and 0.12 for [2], [1], and [3], respectively, which is consistent with our observation that q should be close to zero in order to explain the internal dissipation-free and asymmetric velocity features of the F1 motor.

Let us first consider the large W limit (high ATP concentration). The length scale of potentials $U_n(x) = K(x - nL)^2/2$ and that of $U_n(x) - U_{n+1}(x) = \mp KLx$ are $\sqrt{k_BT/K}$ and k_BT/KL, respectively. Since the potential energy is sufficiently large $KL^2/k_BT \gg 1$, the smallest length scale in this model is $l_v = k_BT/KL$. This length defines the time scale $\tau_v = \Gamma k_BT/(KL)^2$, which determines the typical W (ATP concentration) that allows the effective force description of the model, and consequently the velocity saturation. Let us also define $\tau_p := \Gamma/K$ ($\gg \tau_v$), which corresponds to the time scale of equilibration inside a single potential.

Significance of the time scale τ_v is numerically verified through seeing how the velocity dependence of W in the model changes according to the spring constant K. In Fig. S3, we show the results for the case where K and $\Delta\mu$ are parameterized by d ($= -1, 0, 1, 2, 3, 4, 5$) as

$$KL^2/k_BT = 50 \times 2^{\mathrm{d}} \tag{S13}$$

$$\Delta\mu/k_BT = 19 \times 2^{\mathrm{d}} \tag{S14}$$

Clearly, the value of W at which the velocity saturates is scaled by τ_v ($\propto K^{-2}$) and not by τ_p ($\propto K^{-1}$), when d is sufficiently large.

To understand the limit $W \to 0$ of the model, we focus on the switching dynamics between potentials $U_0(x)$ and $U_1(x) - \Delta\mu$ since the dynamics between two neighboring potentials are equivalent in steady-state. Our aim is to estimate the probability density of the position where the switching from $U_0(x)$ to $U_1(x) - \Delta\mu$ takes place:

$$\lambda_0(x) := \Lambda_0(x)/W = P_0^{ss}(x) f_0^+(x) - P_1^{ss}(x) f_0^-(x). \tag{S15}$$

$P_0^{ss}(x)$ and $P_1^{ss}(x)$ are the steady-state densities of x under the condition that n is 0 and 1, respectively. The first term in the right-hand side of Eq. S15 corresponds to the probability density of the switching at x, whereas the second part is that of the switch back ($1 \to 0$). When $\lambda_0(x)$ is obtained, the internal heat dissipation may be calculated as

$$Q_{\text{int}} = \frac{1}{Z} \int dx\, \lambda_0(x)[U_0(x) - U_1(x) + \Delta\mu] \tag{S16}$$

where $Z = \int dx\, \lambda_0(x)$ is the normalization factor.

For $\ll \tau_p^{-1}$, the steady-state probability density of x is close to the equilibrium density inside each potential

$$P_n^{ss}(x) \simeq P_n^{eq}(x) \propto \exp[-U_n(x)/k_BT] \tag{S17}$$

Although this assumption is valid in estimating the first term in the right-hand side of Eq. S15, it fails to capture the feature of the second term at $W > 0$, since the small but finite switching makes $P_1^{ss}(x)$ deviate from $P_1^{eq}(x)$ at around the peak point of $P_0^{ss}(x) f_0^+(x)$, where $f_0^-(x)$ may take a large value.

We focus on the model with $q < x_c/L$, where $x_c := (KL^2/2 - \Delta\mu)/k_BTKL \simeq 14°$ is the intersection point between the two potentials, $U_0(x_c) - U_1(x_c) + \Delta\mu = 0$. In this region of q, $P_0^{eq}(x) f_0^+(x)$ has a peak at $x < x_c$. In order to phenemenologically take into account the effect of switch back, we consider the conditional probability that after the switching occurs at x, the potential stays as $U_1(x) - \Delta\mu$ and is not switched back to $U_0(x)$:

$$D_0(x) := \frac{\exp[-\tau_v/\tau_{leq}(x)] + \exp[E_0(x)]}{1 + \exp[E_0(x)]} \tag{S18}$$

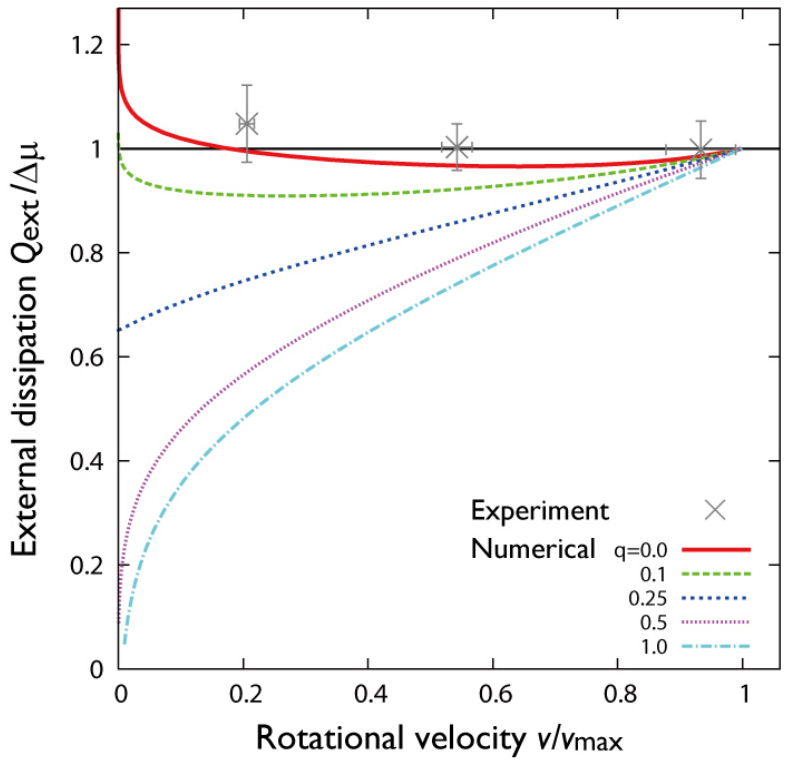

FIGURE S2 Rotational velocity v versus the external heat dissipation per step Q_{ext} in the harmonic potential model. Parameters are given in the text. The experimental results were obtained from [5] (error bar: standard error of mean).

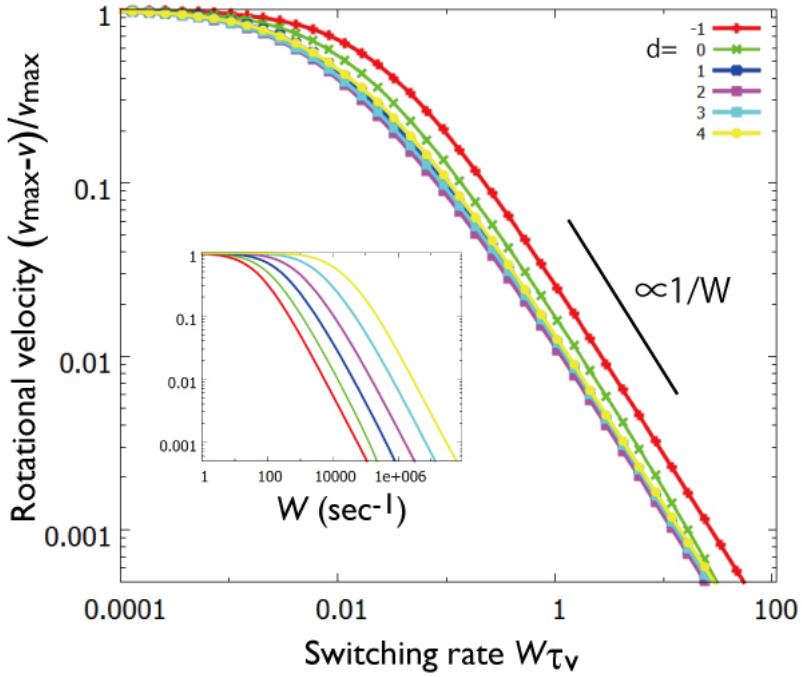

FIGURE S3 W dependence of velocity for the harmonic potential model with $q = 0$ (numerical). Different colors correspond to different d's, which changes the set of spring constant K and hydrolysis free energy $\Delta\mu$ in the model according to Eqs. S13 and S14. Results from models with different d are plotted by scaling W by τ_v^{-1}. Inset shows same data without scaling W.

We have introduced the local equilibrium time scale

$$\tau_{leq}(x) := \frac{1}{R_0^+(x) + R_0^-(x)} = \frac{1}{W[f_0^+(x) + f_0^-(x)]} \tag{S19}$$

which is the typical time required for equilibration between $U_0(x)$ and $U_1(x) - \Delta\mu$ at a fixed position x. Using $D_0(x)$, we assume that the switching position probability density is given by

$$\tilde{\lambda}_0(x) := P_0^{eq}(x) f_0^+(x) D_0(x) \tag{S20}$$

This is justified since the main contribution from the $P_1^{ss}(x) f_1^-(x)$, term in Eq. S15 is the switch back which occurs right after the switch $0 \to 1$, and the probability that the probe spontaneously climbs the potential $U_1(x)$ in the backward direction for the switch back to occur is negligibly small. As shown in Fig. S4, the external heat dissipation theoretically obtained as

$$\tilde{Q}(W) := \Delta\mu - \frac{1}{Z}\int dx\, \lambda_0(x)[U_0(x) - U_1(x) + \Delta\mu] \tag{S21}$$

$$= \frac{1}{2}KL^2 - KL\frac{1}{Z}\int dx\, \lambda_0(x) x \tag{S22}$$

captures the feature of Q_{ext} at small W. Note that in the limit $W \to 0$, we find

$$Q_{\text{ext}} = \tilde{Q}(W = 0) = \left(\frac{1}{2} - q\right)KL^2 \tag{S23}$$

since in this limit the switching position probability density becomes $P_0^{eq}(x) f_0^+(x) \propto \exp[-K(x - qL)^2/2k_BT]$, a Gaussian distribution with peak at $x = qL$. For finite W, the value of Q_{int} deviates drastically from $\tilde{Q}(W = 0)$ in a manner $\propto -\log W$, which is observed as a sharp drop when W or v is linear scaled (Fig. S4 inset, Fig. S2). Physically, this corresponds to the fact that very little ADP concentration is sufficient to prevent switching to occur at energetically unfavorable positions $[U_0(x_c) - U_1(x_c) + \Delta\mu \gg k_BT]$.

$\lambda_0(x) \simeq \tilde{\lambda}_0(x)$ is valid when $W \ll \tau_p^{-1}$, and should fail when $W > \tau_p^{-1}$ since Eq. S17 used to evaluate the first term of Eq. S15 is violated in this region. The Q_{ext} therefore deviates from the sharp theoretical curve at around $W \simeq \tau_p^{-1}$ (Fig. S5). As shown in Fig. S4, the value of $\tilde{Q}(W)$ is sufficiently close to $\Delta\mu$ when $W \simeq \tau_p^{-1}$, which could be understood as follows. Assuming $D_0(x) \simeq \exp[-\tau_v/\tau_{leq}(x)]$, the peak position $x = x_c - \delta$ of $\Lambda_0(x)$ at $W = \tau_p^{-1}$ satisfies

$$\frac{KL(x_c - qL)}{k_BT} = \frac{KL\delta}{k_BT} - q\exp\left[\frac{qKL\delta}{k_BT}\right] + (1 - q)\exp\left[\frac{(1 - q)KL\delta}{k_BT}\right] \tag{S24}$$

Using the δ obtained in Eq. S24, $\tilde{Q}\left(W = \tau_p^{-1}\right)$ is estimated as $\simeq \Delta\mu + KL\delta$. At large $A := KL^2/k_BT$ and $B := \Delta\mu/k_BT = O(A)$, the value of δ satisfying Eq. S24 scales as $A\delta/L \propto \log A$. Therefore, $\tilde{Q}\left(W = \tau_p^{-1}\right)/\Delta\mu = 1 + O(\log A/A)$, which means that $\tilde{Q}\left(W = \tau_p^{-1}\right) \simeq \Delta\mu$ is satisfied with a small error term under $A \gg 1$.

To sum up, in the potential switching model with the switching rates (3) and (4) in the main text and $q < x_c/L$, Q_{ext} becomes sufficiently close to $\Delta\mu$ at $W \simeq \tau_p^{-1}$, when the condition $KL^2, \Delta\mu \gg k_BT$ is satisfied. Since $\tau_p = \tau_v KL^2/k_BT$, there exists a time scale separation $\tau_p \gg \tau_v$, hence at $W \simeq \tau_p^{-1}$ the velocity is still smaller than the maximum velocity, $v < v_{\max}$. This means that if $KL^2/k_BT = 50$, which is the case where the maximum velocity is close to the real F_1, the model shows the $Q_{\text{ext}} \sim \Delta\mu$ behavior even when [ATP] is as low as 1/50 of the velocity saturating concentration. Persistent $Q_{\text{ext}} \sim \Delta\mu$ for the broad range of $W > \tau_p^{-1}$ allows the low dependence of Q_{ext} on v, which explains the internal dissipation-free feature of F_1 observed in experiment. For the case of models with $q > x_c/L$, it is confirmed that there exists a significant difference between Q_{ext} and $\Delta\mu$ for $= \tau_p^{-1}$, even when d is as large as 5 in the parameterization given by Eqs. S13 and S14. It is left for future studies to theoretically understand the $q > x_c/L$ models (including $q = 0.5$ and 1, Fig. S6).

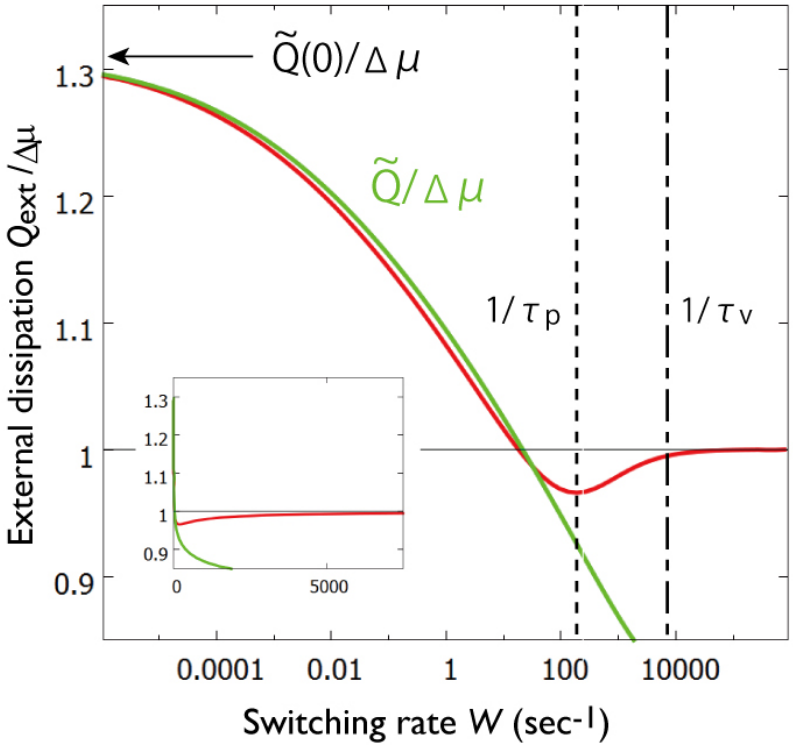

FIGURE S4 Numerically obtained Q_{ext} (red) and the theoretical $\tilde{Q}(W)$ (green) obtained from Eq. S22 in the $q = 0$ model. Starting from $\tilde{Q}(0)$ in the limit $W \to 0$, Q_{ext} drops sharply in a manner $\propto -\log W$ at low but finite W. Q_{ext} stops dropping at $W \simeq \tau_p^{-1}$, and converges to $\Delta\mu$ at $W > \tau_p^{-1}$. Inset shows same data with linear-scale W.

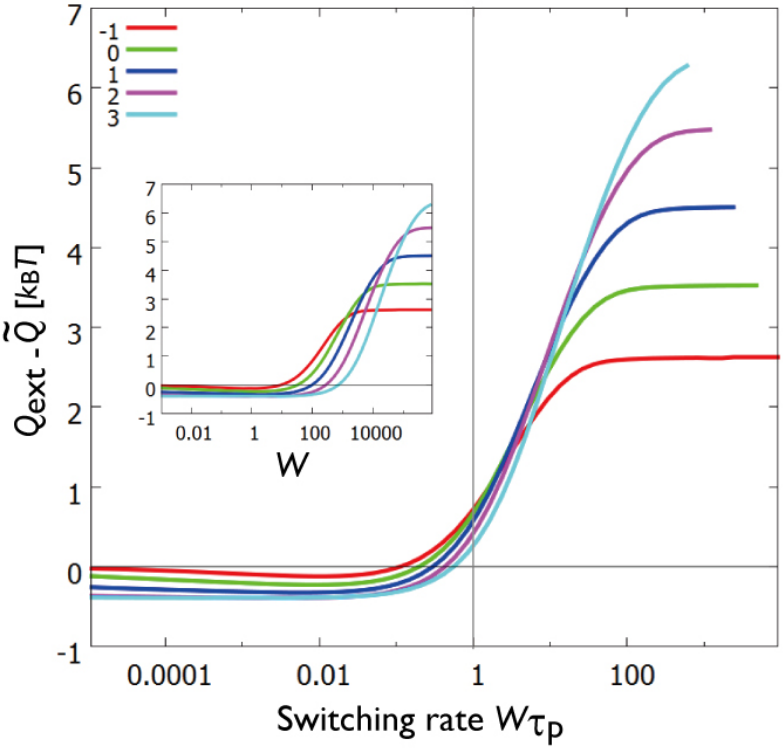

FIGURE S5 Deviation of Q_{ext} from the theoretically obtained $\tilde{Q}(W)$ from Eq. S22. Different colors correspond to $d = -1, 0, 1, 2, 3, 4, 5$ in the model parameterized by Eqs. S13 and S14. Inset shows same data without scaling.

C. External torque dependence of velocity in various models

In Fig. S8, the external torque dependence of the rotational velocity for the $q = 0.5$ (left) and 1 (right) models are shown. We used Eq. S7 for $U_0(x)$, with $k = 0.0061\ \mathrm{deg}^{-2} k_B T$. and $\tilde{\Delta\mu} = 5.2\ k_B T$. In comparison to the $q = 0$ model (Fig. 5A in main text), the $q = 0.5$ and 1 models fail to capture the feature of F_1, where large minus velocity in the presence of large torque and low nucleotide concentration has been observed. Notice that in the case of $q = 0.5$, the curves are close to anti-symmetric in a wide range of W [represented by $v(0)$].

We define the intersection switching model by

$$f_n^+(x) = \exp\left[-\frac{(x - x_{c,n})^2}{2\sigma^2} + \frac{q}{k_B T}\left[U_n(x) - U_{n+1}(x) + \Delta\mu\right]\right],$$
$$f_{n+1}^-(x) = \exp\left[-\frac{(x - x_{c,n})^2}{2\sigma^2} + \frac{q-1}{k_B T}\left[U_n(x) - U_{n+1}(x) + \Delta\mu\right]\right], \quad \text{(S25)}$$

Here, $x_{c,n}$ is the intersection point between the two potentials $U_n(x)$ and $U_{n+1}(x) - \Delta\mu$, satisfying $U_n(x_{c,n}) - U_{n+1}(x_{c,n}) + \Delta\mu = 0$, and σ is the typical width of the window of the angle at which the switching is allowed. If σ is sufficiently small, this model would become internal dissipation-free for a wide range of W, which seems to explain the experimental data. This is because the switching of the mechanical potential only occurs at angles satisfying $U_n(x) - U_{n+1}(x) + \Delta\mu \simeq 0$ in this model. However, if σ is too small, the torque dependence of the velocity becomes anti-symmetric with respect to the $F = \Delta\mu/L$ line for all q even at small W (Fig. S8 left), which is inconsistent with the experimental observations. When σ is sufficiently large (Fig. S8 right), the torque-velocity curve would depend on q, which shows that adopting $q \simeq 0$ is critical even in the intersection switching model to reproduce the feature of F_1.

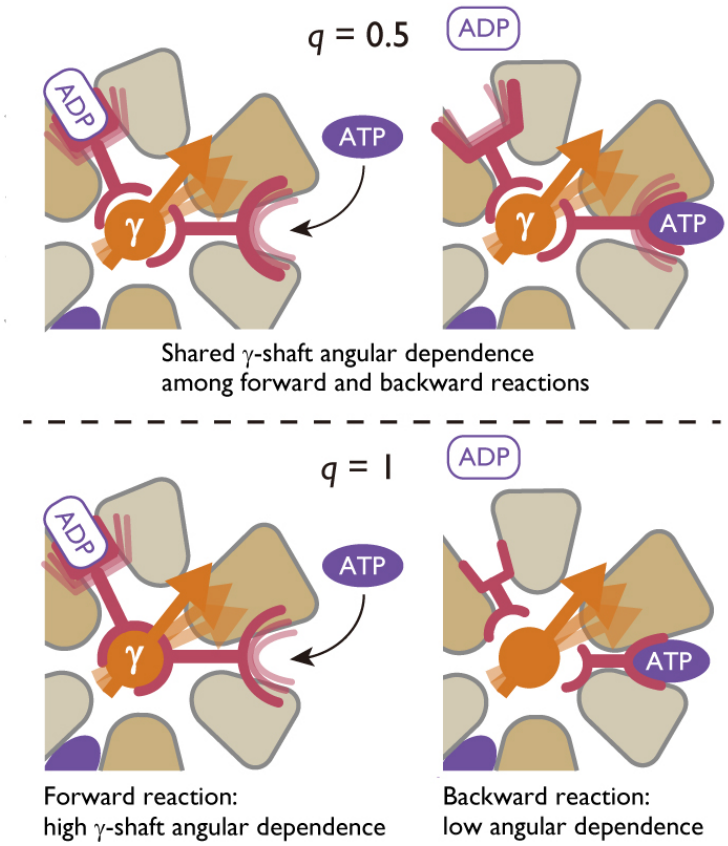

FIGURE S6 Schematic of the $q = 0.5$ and $q = 1$ models. In the $q = 0.5$ model, the coordination between the γ shaft and the nucleotide binding sites are equally present in the forward and backward reactions. On the other hand, the γ shaft and the nucleotide binding sites are only coordinated in the forward step in the $q = 1$ model, which is completely opposite to the case of $q = 0$ model (Fig. 1*B* in the main text). As shown in Fig. 2*C* and 3*A* in the main text, these models fail to reproduce the internal dissipation-free feature of F_1.

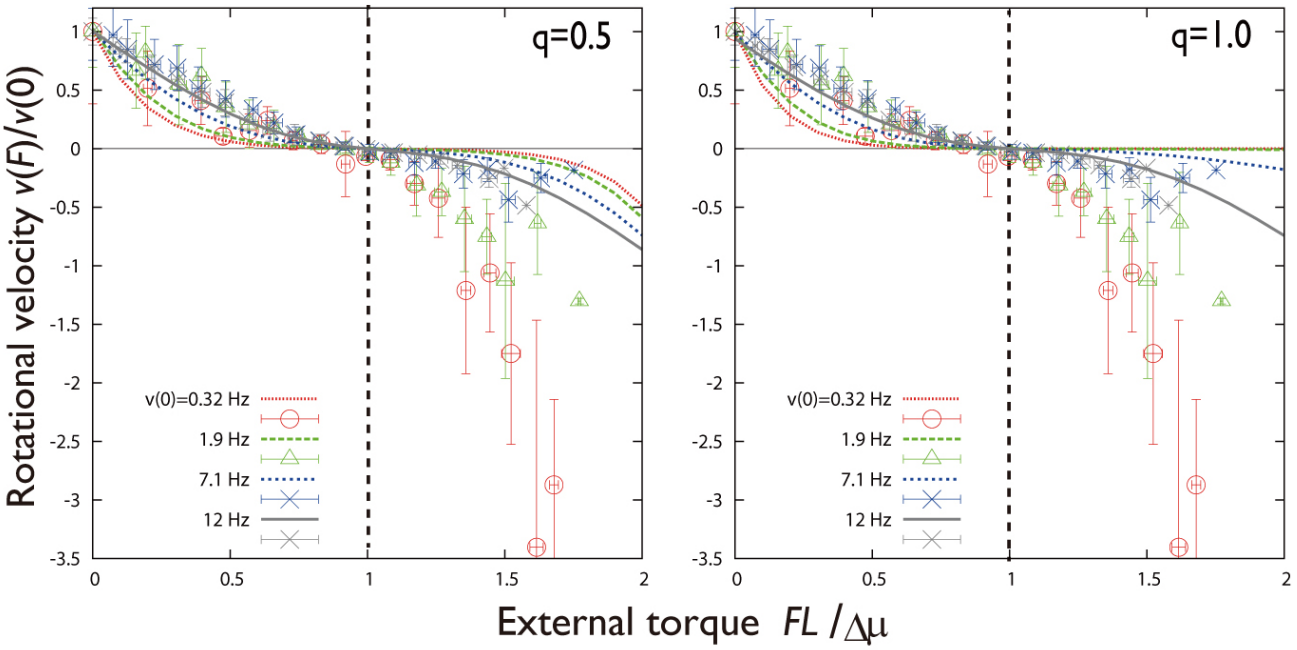

FIGURE S7 External torque dependence of the rotational velocity in the $q = 0.5$ (left) and 1.0 (right) models, plotted with the experimental data [6] (kindly provided by S. Toyabe). For each numerical lines, W was chosen and fixed in order to reproduce the values of $v(0)$ of the corresponding experimental data.

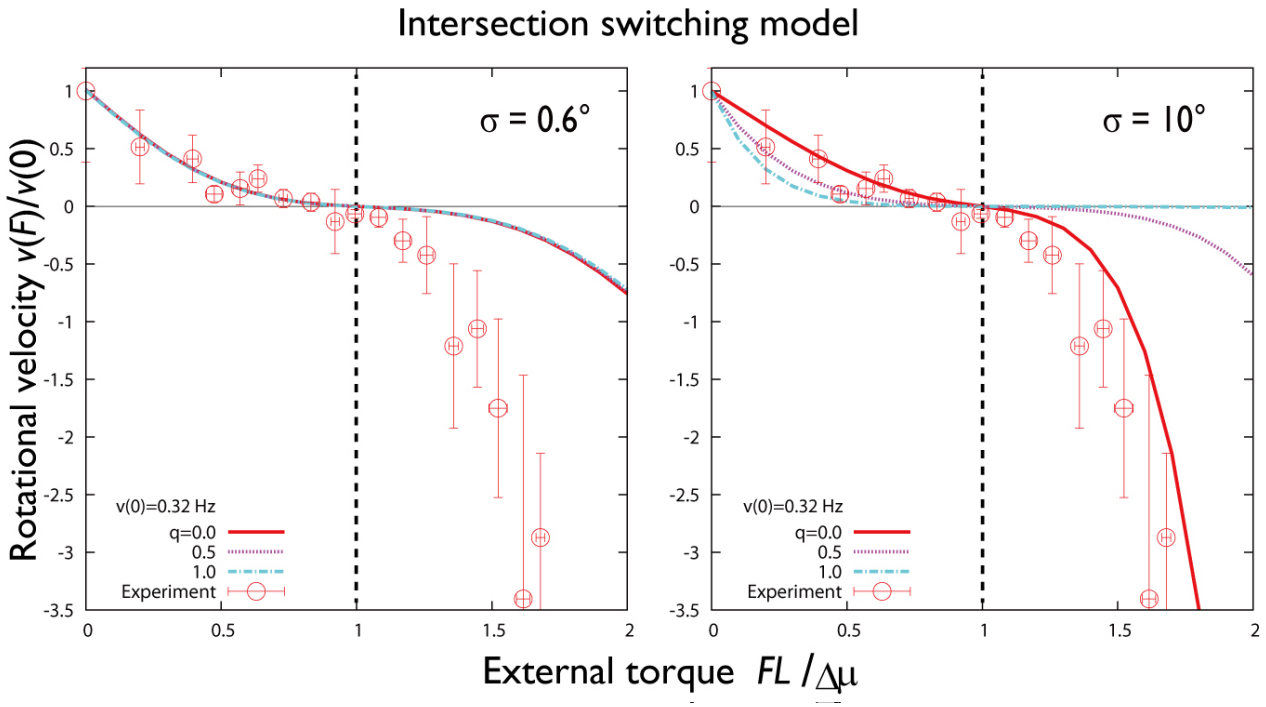

FIGURE S8 External torque dependence of the rotational velocity for the intersection switching model [see text Eq. S25]. When σ is small and the switching is only allowed in a narrow range around the potential intersection point (left), the torque-velocity curve becomes anti-symmetric with respect to the $FL = \Delta\mu$ line. When σ is set larger (right), the q-dependence appears. For each numerical lines, W was chosen and fixed in order to reproduce the values of $v(0) = 0.32$ Hz.

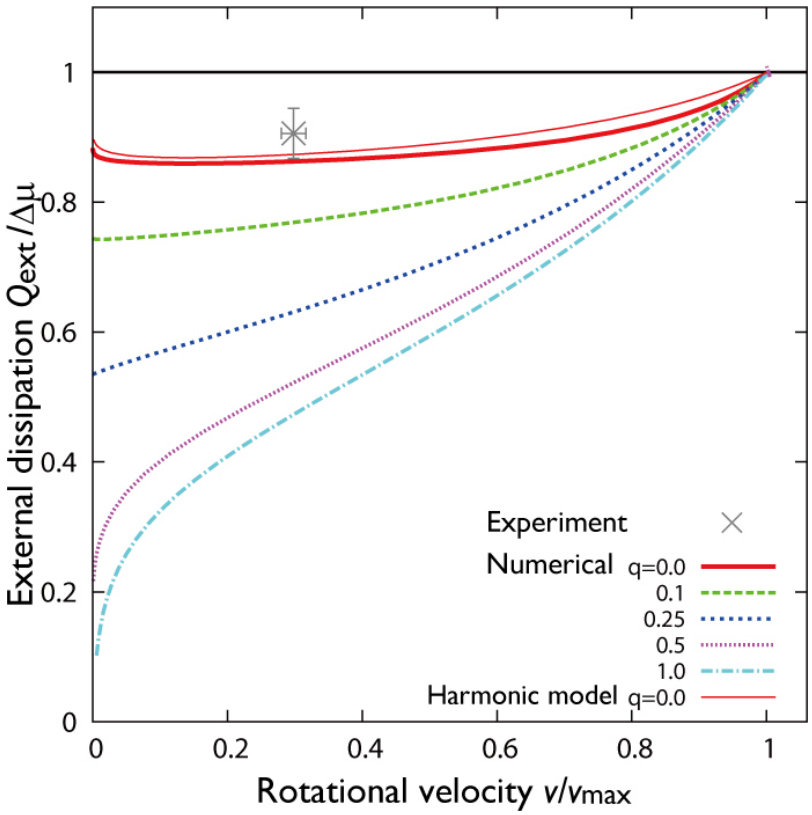

FIGURE S9 Rotational velocity v versus the external heat dissipation per step Q_{ext} in the non-harmonic potential model [using Eq. S7 for $U_0(x)$], and the harmonic potential model, in the case of $\Delta\mu = 28\, k_B T$. Parameters from Supplementary Material A and B were used. The experimental result was obtained from [5] (error bar: standard error of mean). In this large $\Delta\mu$ setup, the intersection point becomes $x_c < 0$ in the non-harmonic and harmonic potentials we have introduced. Nevertheless, numerical result for $q = 0$ shows consistent value with experiment.

SUPPORTING REFERENCES

[1] Watanabe R et al. (2012). Mechanical modulation of catalytic power on F1-ATPase. *Nat. Chem. Biol.* 8:86–92.

[2] Iko, Y et al. (2009). Acceleration of the ATP-binding rate of F1-ATPase by forcible forward rotation. *FEBS lett.* 583:3187–3191.

[3] Adachi, K et al. (2012). Controlled rotation of the F1-ATPase reveals differential and continuous binding changes for ATP synthesis. *Nat. Commun.* 3:1022–1033.

[4] Toyabe S, Ueno H, & Muneyuki E (2012). Recovery of state-specific potential of molecular motor from single-molecule trajectory. *Euro. Phys. Lett.* 97:40004–40009.

[5] Toyabe S et al. (2010). Nonequilibrium energetics of a single F1-ATPase molecule. *Phys. Rev. Lett.* 104:198103–198106.

[6] Toyabe S et al. (2011). Thermodynamic efficiency and mechanochemical coupling of F1-ATPase. *Proc. Natl. Acad. Sci.* 108:17951–17956.